

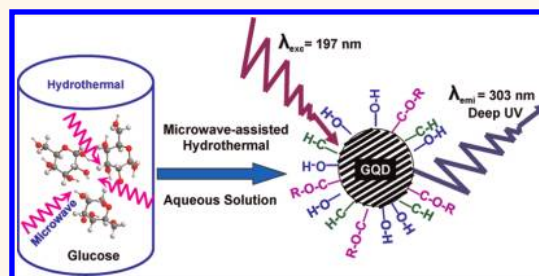
# Deep Ultraviolet Photoluminescence of Water-Soluble Self-Passivated Graphene Quantum Dots

Libin Tang,<sup>†,\*</sup> Rongbin Ji,<sup>‡</sup> Xiangke Cao,<sup>§</sup> Jingyu Lin,<sup>§</sup> Hongxing Jiang,<sup>§</sup> Xueming Li,<sup>||</sup> Kar Seng Teng,<sup>⊥</sup> Chi Man Luk,<sup>†</sup> Songjun Zeng,<sup>†</sup> Jianhua Hao,<sup>†</sup> and Shu Ping Lau<sup>†,\*</sup>

<sup>†</sup>Department of Applied Physics, The Hong Kong Polytechnic University, Hong Kong SAR, <sup>‡</sup>Kunming Institute of Physics, Kunming, 650223, Yunnan Province, P.R. China, <sup>§</sup>Department of Electrical and Computer Engineering, Texas Tech University, Lubbock, Texas 79409, United States, <sup>||</sup>Solar Energy Research Institute, Yunnan Normal University, Kunming 650092, P.R. China, and <sup>⊥</sup>Multidisciplinary Nanotechnology Center, College of Engineering, University of Swansea, Singleton Park, Swansea SA2 8PP, United Kingdom

Graphene quantum dots (GQDs) have attracted great attention for their unique spin,<sup>1,2</sup> electronic,<sup>3</sup> and optical properties.<sup>3–10</sup> Several approaches have been developed to fabricate GQDs, such as hydrothermal graphene oxide reduction,<sup>4,11,12</sup> bottom-up synthesis,<sup>8</sup> electrochemical<sup>9</sup> and metal-catalyzed<sup>13</sup> approaches, chemical synthesis,<sup>14,15</sup> chemical exfoliation,<sup>16</sup> and electron beam lithography.<sup>17</sup> Although most of the so-called GQDs are not monolayer in nature, the term usually represents few layers to tens of layers of graphene with a size less than 30 nm.<sup>4,5,7–11</sup> In recent years, a microwave pyrolysis method has been developed to prepare carbon nanoparticles,<sup>18,19</sup> with particle size ranging from 1 to 5 nm, but no crystalline quantum dots have been observed in the absence of additives. Nanostructured carbons have also been called carbon nanoparticles (CNPs),<sup>18</sup> or more simply carbon dots (CDs),<sup>19</sup> because of their amorphous nature. However similar to GQDs, these carbon-based nanomaterials exhibited color-tunable photoluminescence properties with emission wavelengths covering the visible spectrum. It will be of scientific and technological importance if GQDs can emit deep ultraviolet (DUV) wavelength. Here, we report the first observation of DUV emission at 303 nm ( $\sim 4.1$  eV) from the GQDs when excited by a 197 nm laser. This is the shortest emission wavelength reported from solution-based inorganic and organic QDs. In addition, the structural and chemical information of the GQDs were studied by employing electron energy loss spectroscopy (EELS). It revealed that the GQDs are composed of  $sp^2$  bonded carbon (C=C) and surface passivated C–O based functional

## ABSTRACT



Glucose-derived water-soluble crystalline graphene quantum dots (GQDs) with an average diameter as small as 1.65 nm ( $\sim 5$  layers) were prepared by a facile microwave-assisted hydrothermal method. The GQDs exhibits deep ultraviolet (DUV) emission of 4.1 eV, which is the shortest emission wavelength among all the solution-based QDs. The GQDs exhibit typical excitation wavelength-dependent properties as expected in carbon-based quantum dots. However, the emission wavelength is independent of the size of the GQDs. The unique optical properties of the GQDs are attributed to the self-passivated layer on the surface of the GQDs as revealed by electron energy loss spectroscopy. The photoluminescence quantum yields of the GQDs were determined to be 7–11%. The GQDs are capable of converting blue light into white light when the GQDs are coated onto a blue light emitting diode.

**KEYWORDS:** graphene · quantum dots · deep ultraviolet · fluorescence · self-passivated · graphene quantum dots

groups. Our study may open up new avenues for developing DUV photonic devices using GQDs as the active material.

## RESULTS AND DISCUSSION

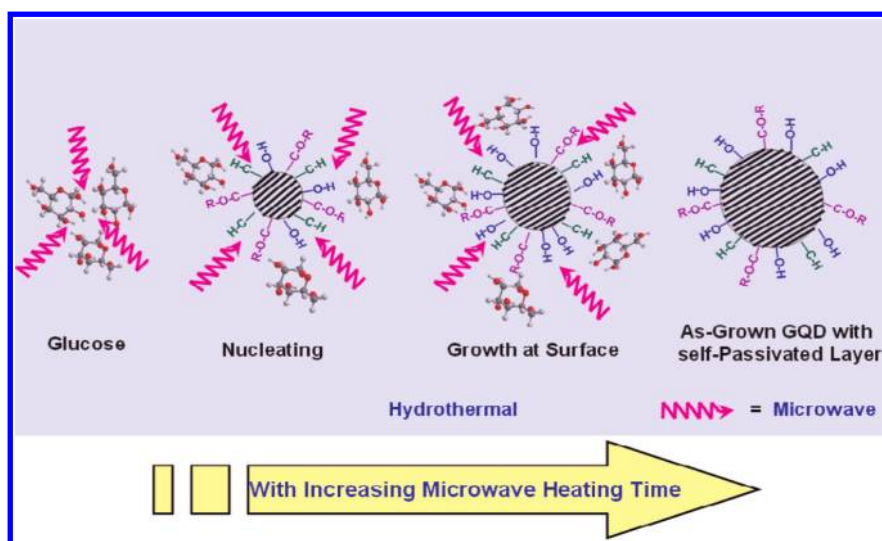
The GQDs were prepared by a microwave-assisted hydrothermal (MAH) method that combined both the advantages of hydrothermal and microwave techniques. The microwave heating provides simultaneous, homogeneous, and fast heating, leading to uniform size distribution of quantum dots. Furthermore, this MAH

\* Address correspondence to [apsplau@polyu.edu.hk](mailto:apsplau@polyu.edu.hk).

Received for review February 20, 2012 and accepted May 5, 2012.

Published online May 05, 2012  
10.1021/nn300760g

© 2012 American Chemical Society



Scheme 1. Preparation of GQDs by MAH method.

method does not require any surface passivation agents or inorganic additives. The sole reagent is glucose (sucrose or fructose), which makes this method attractive as compared to other GQD synthesis methods. As shown in Scheme 1, the glucose molecules are pyrolyzed and then converted to GQDs. On the basis of our experiments, we deduced that most of the carbohydrates which contain C, H, and O in the ratio of  $\sim 1:2:1$  may be used as the carbon source to prepare GQDs provided that H and O exist in the forms of hydroxyl, carboxyl, or carbonyl groups that may dehydrate under hydrothermal conditions. Since glucose-, sucrose-, and fructose-derived GQDs exhibited similar properties, as a typical example, we present the results based on glucose derived GQDs throughout this paper unless otherwise indicated.

Figure 1a shows the transmission electron microscopy (TEM) image of the monodispersed GQDs. The high-resolution TEM (HRTEM) images, as shown in Figures 1b–d and Figure S1 of the Supporting Information (SI), reveal the high crystallinity of the GQDs. The lattice parameter of 0.352 nm as shown in Figure 1b is the  $d$  spacing between graphene layers, taking into account that the basal plane distance of bulk graphite is 0.335 nm.<sup>20,21</sup> The X-ray diffraction (XRD) patterns of the GQDs prepared at various heating times are shown in Figure S2 of SI. The diffraction peak is in the range of  $18.42\text{--}25.92^\circ$  which corresponds to a graphitic structure. The peak is broad due to the small size of the GQDs. The calculated  $d$  spacing ranges from 0.343 to 0.481 nm. The values are in good agreement with the reported values (0.340–0.403 nm) of GQDs prepared by other methods.<sup>4,9,16</sup> The small difference in  $d$  spacing between the bulk graphite and the GQDs is attributed to the presence of  $-\text{O}-\text{H}$ ,  $-\text{C}-\text{H}$ , and  $-\text{C}-\text{O}-\text{R}$  at the edges of the GQDs that enlarges the spacing of graphene layers. Figure 1c shows a single GQD of diameter 3.39 nm with an in-plane lattice spacing of 0.214 nm.

The corresponding selected area fast Fourier transform (FFT) image is shown in the inset of Figure 1d, revealing the lattice fringes and number of graphene layers ( $\sim 10$ ) in the GQD. The  $[110]$  and  $[1\bar{1}0]$  planes correspond well to graphite. Both the basal and in-plane lattice parameters indicate that the GQDs exhibit graphitic structure rather than diamond structure. Figure 1e shows the size distribution of the GQDs corresponding to the sample as shown in Figure 1a. The average diameter of the GQDs is  $3.4 \pm 0.5$  nm and the size distribution accords well with Gaussian distribution. The full-width-at-half-maximum (fwhm) of the fitted Gaussian curve is 0.55 nm, indicating the narrow distribution nature of the GQDs. Figure 1f shows the atomic force microscopy (AFM) image of the monodispersed GQDs, four GQDs are selected randomly and labeled as 1, 2, 3, and 4. The average height of these GQDs is 3.2 nm as shown in Figure 1g. The monodispersed property of the GQDs could be attributed to the rapid, simultaneous, homogeneous heating of the solvent ( $\text{H}_2\text{O}$ ) and glucose by microwave irradiation, which provides uniform nucleation and growth of the GQDs. The diameter of the GQDs can be increased by increasing microwave heating time. Figure 1h shows the average diameter of the GQDs determined by TEM as a function of heating time. The size of the GQDs can be tuned from 1.65 to 21 nm by simply prolonging the heating time from 1 to 9 min, respectively. The diameter of the GQDs increases rapidly with increasing heating time. The TEM images and size distribution of the samples prepared at 1 and 9 min are shown in Figures S1 and S3 of SI. The average sizes of the GQDs as determined by TEM are consistent with the AFM results (Figure 1f and Figure S4 of SI). Interestingly, few-layer ( $\leq 10$ ) GQDs can be obtained if the heating time is less than 5 min.

Electron energy loss spectroscopy (EELS)<sup>22</sup> is a powerful tool to characterize the chemical composition and structure of carbon-based materials. Figure 2a

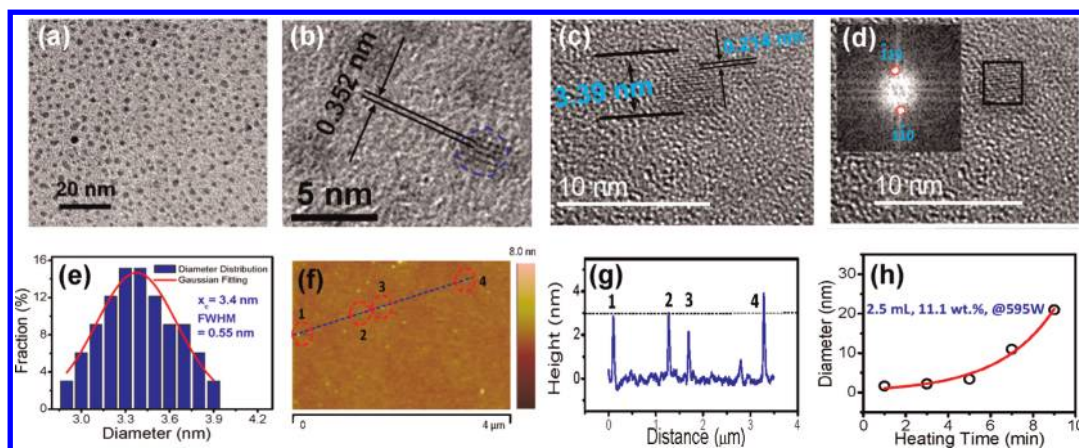


**Figure 1.** TEM and AFM images of the GQDs. (a) TEM image of the GQDs assembled on Cu grid coated with ultrathin amorphous carbon film; (b) the HRTEM image of the GQDs; (c) a typical single GQD, the size and its lattice parameter are 3.39 and 0.214 nm, respectively; (d) HRTEM image of a typical single GQD, and its corresponding selected area FFT image (inset); (e) the diameter distribution of the GQDs, the red line is the Gaussian fitting curve; (f) AFM image of the GQDs; (g) the height distribution of the GQDs as shown in AFM image f; (h) the GQDs diameter dependent on heating time. The GQDs were prepared using 11.1 wt % glucose solution and 5 min (except for panel h) microwave heating at 595 W.

shows that energy loss spectrum of the GQDs. EELS spectra of C K-edge (285 eV) and O K-edge (539 eV) are shown in the insets of Figure 2a. The peak at 285 eV is attributed to the transition from  $1s \rightarrow \pi^*$  state ( $1s \rightarrow \pi^*$ ), and the peak at 291 eV is the transition from  $1s \rightarrow \sigma^*$  state ( $1s \rightarrow \sigma^*$ ). These are the main EELS features of  $sp^2$  bonded (C=C) carbon at the K-edge region.<sup>23</sup> The peak at 539 eV is caused by  $1s \rightarrow \sigma^*$  of C–O.<sup>24</sup> This indicates that GQDs are self-passivated with O-related functional groups. Scanning transmission electron microscopy (STEM) and energy dispersive X-ray spectroscopy (EDS) were employed to analyze the elemental distribution of the GQDs. Figure 2b shows the dark field image of the GQDs. The corresponding elemental C and O mappings are shown in Figure 2 panels c and e, respectively. Evidently, the content of C is more than that of O. The atomic ratio of C/O is 95.4/4.6 as calculated from the EDS spectrum as shown in Figure 2d. C is the dominate element in the GQDs.

Fourier transform infrared (FTIR) spectroscopy was used to investigate the bonding composition of the GQDs and its functional groups. Figure 3a shows the FTIR spectra of the GQDs prepared by various source concentrations and microwave heating times. An obvious absorption peak centered at  $1641 \text{ cm}^{-1}$ , which is caused by C=C stretching, is observed. Under the MAH process, glucose is dehydrated to form C=C which is the elementary unit of the GQDs. A sharp absorption peak at  $852 \text{ cm}^{-1}$  from the source glucose is due to  $\text{CH}_2$  rocking. Such a peak becomes much weaker from the GQDs spectrum, indicating a drastic decrease in H after the formation of GQDs. The broad peak centered at  $3392 \text{ cm}^{-1}$  reveals O–H bonding. The absorptions at  $1027$  and  $1076 \text{ cm}^{-1}$  are attributed to  $\nu_{\text{C-O}}$ ; absorptions at  $1360$  and  $2927 \text{ cm}^{-1}$  also reveal the existence of C–H.

To further confirm the functional groups on the surface of the as-prepared GQDs, we carried out X-ray

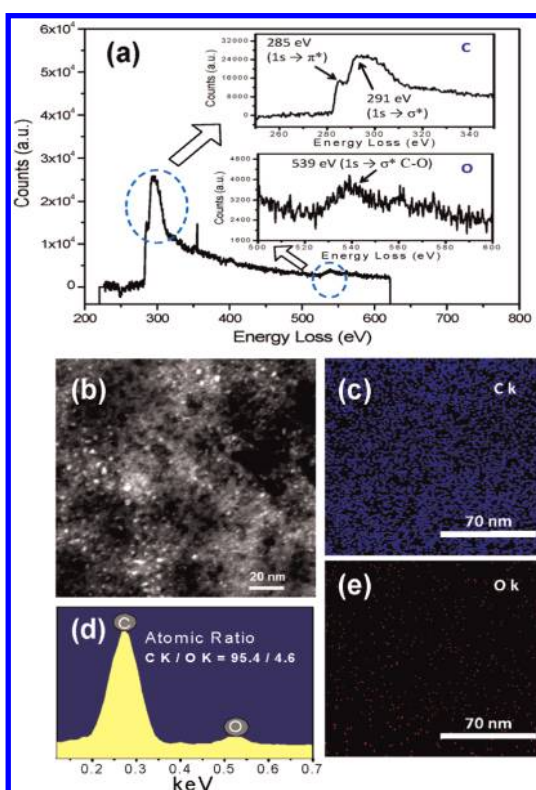


**Figure 2.** EELS spectra, STEM image, and EDS analysis of the GQDs. (a) EELS spectrum of the GQDs; the insets show the EELS spectra of C K-edge and O K-edge of the GQDs; (b) STEM image of the GQDs assembled on Cu grid coated with ultrathin amorphous carbon film; (c) Elemental C mapping (in blue) of the image shown in panel b; (d) EDS spectrum of the GQDs; (e) elemental O mapping (in red) of the image shown in panel b. The GQDs were prepared using 11.1 wt % glucose solution and 7 min microwave heating at 595 W.

photoelectron spectroscopy (XPS) characterization. Figure 3b shows the XPS spectrum of C1s. The measured spectrum can be deconvoluted into five surface components, corresponding to  $sp^2$  (C=C) at binding energy

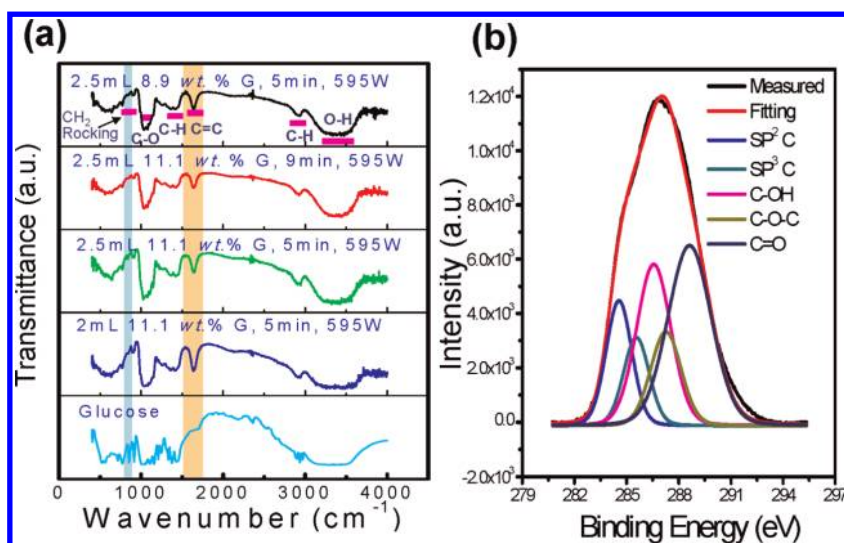


Figure 3. (a) FTIR spectra of the source glucose and the GQDs prepared under different conditions. All the GQDs prepared under different conditions show similar IR absorption peaks. The absorption at  $1641\text{ cm}^{-1}$  is attributed to the formation of C=C which is the typical and main component of the GQDs, and it is absent from the source. (b) The C1s XPS spectrum of the GQDs. The GQDs were prepared with 11.1 wt % glucose solution for 9 min at 595 W microwave heating.

of 284.5 eV,  $sp^3$  (C–C, and C–H) at 285.5 eV, C–OH at 286.6 eV, C–O–C at 287.2 eV, as well as C=O at 288.6 eV. It should be noted that the XPS data presented here represent the surface components of the GQDs, thus the relative contents of the core component (C=C) of the GQDs cannot be obtained. The surface components of the GQDs as determined by the XPS are in good agreement with FTIR results.

As mentioned before, the size of the GQDs increases with increasing microwave heating time. The proposed mechanism is schematically shown in Scheme 1. First glucose molecules are dehydrated to form the nucleus of GQDs that is composed of C=C as revealed by HRTEM, EELS, FTIR, and XPS. Then the growth of GQD occurs at the spherical surface (edge growth), with increasing heating time. The source molecules reach the surface of the GQD and generate new C=C by dehydration. By this way GQD becomes larger as heating time increases. Owing to the high pressure induced by the hydrothermal condition, the freshly formed C=C is orderly arranged and assists the growth of crystalline GQDs. The functional groups (–O–H, –C–H, and –C–O–R) located at the surface of the GQDs act as a “passivation” layer for the GQDs. This self-passivated layer on the surface of the GQDs facilitates the solubility of GQDs in water as well as the efficient photoluminescence properties which will be discussed later.

As shown in Figure 4a the absorbance decreases as dilution fold increases, maintaining similar absorption spectra. Two deep UV absorption peaks centered at 228 and 282 nm are observed for all the GQD samples. The linear relationships between the absorbance and 1/dilution times for the two peaks 228 and 282 nm are shown in the inset of Figure 4a. Since the as-prepared

GQDs showed saturated absorption in the deep UV range, the samples were diluted by water in order to explore the intrinsic deep UV absorption. The absorbance of the GQDs was determined by multiplying the dilution times from the absorbance of the diluted GQD solutions.

Interestingly, both intensities of the two deep UV absorbance peaks at 228 and 282 nm increase exponentially as the microwave heating time increases as shown in Figure 4b. The GQD samples were derived from 11.1 wt % glucose solution. The intensity ratio between the absorbance peaks 282 and 228 nm as a function of the heating time is shown in Figure 4c. For the heating time below 4 min, the 228 nm absorbance peak is stronger than that of 282 nm. However when the heating time exceeds 4 min, the absorbance peak at 282 nm becomes more intense than that of 228 nm. A linear relationship between the absorbance ratio of the two deep UV peaks and the heating time is observed. The absorption peaks at 228 and 282 nm of the GQD samples are similar to GQDs prepared from hydrothermal graphene oxide reduction method (230 and 320 nm).<sup>4</sup> The origin of these peaks is related to  $\pi$  electron transition in oxygen-containing GQD. The absorption peak at 228 nm is due to  $\pi \rightarrow \pi^*$  of C=C, and the absorption at 282 nm corresponds to  $n \rightarrow \pi^*$  transition of the C=O bond.<sup>25</sup>

Many parameters may affect the growth of the GQDs which include source concentration, microwave power and heating time. The effect of heating time on the absorbance of the GQDs is shown in Figure 4d. All the GQDs show two obvious absorption peaks centered at 228 and 282 nm. It is worth noting that the absorption edges red-shifted while the peak positions remain unchanged as heating time increased. As mentioned

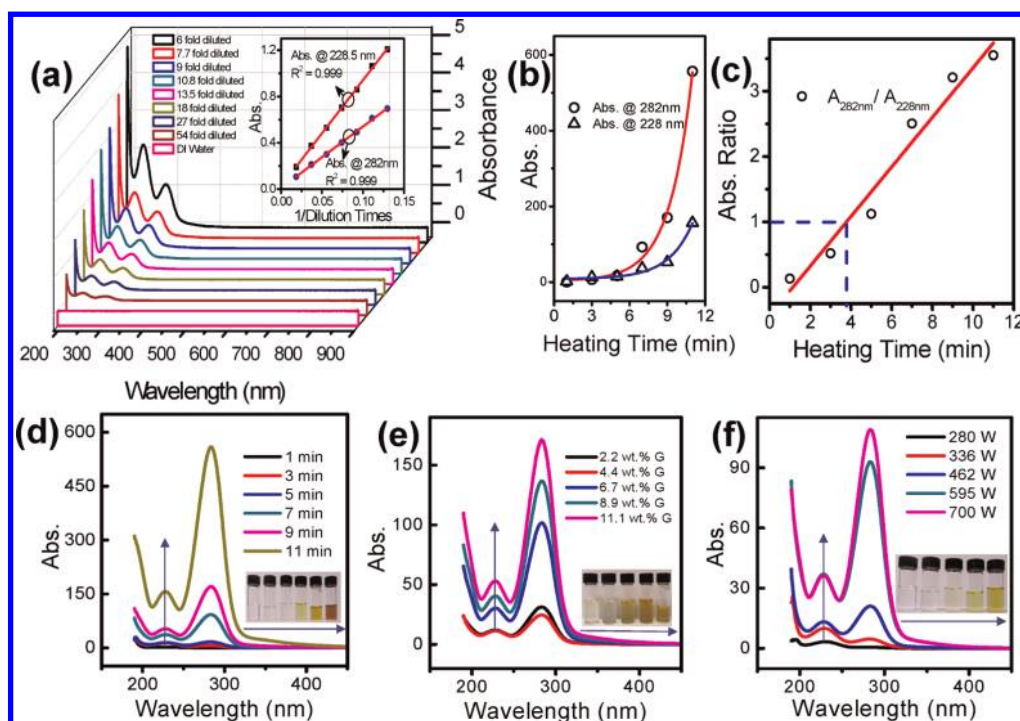


**Figure 4.** Deep UV absorption of the GQDs. (a) The deep UV absorptions of the GQDs with different folds of dilution; the inset is the linear relationship between absorbance (at 228 and 282 nm, respectively) and 1/dilution time; (b) the exponential relationships between the absorbance (at 228 and 282 nm) and microwave heating time; (c) the linear relationship between the absorbance ratio of 282–228 nm and microwave heating time; (d) the effect of microwave heating time on the absorbance of the GQDs prepared at 595 W; (e) the effect of source concentration on the absorbance of the GQDs for microwave heating of 9 min at 595 W; (f) the effect of microwave power on the absorbance of the GQDs heated for 7 min at 280, 336, 462, 595, and 700 W. The insets in panels d–f are the corresponding solutions under ambient light.

before, the size of the GQDs can be increased with increasing heating time. Surprisingly, the two absorption peaks are independent of the size of the GQDs which is different from most of the inorganic semiconductor QDs such as CdS,<sup>26</sup> InAs,<sup>27</sup> InP,<sup>28</sup> PbS,<sup>29</sup> PbSe,<sup>30</sup> and HgTe.<sup>31</sup> When the GQDs are prepared by increasing the source concentration and microwave heating time, in general the intensity of the two absorbance peaks increase without changing the peak position, but are accompanied by a red-shifted absorption edge as shown in Figure 4e,f. The corresponding pictures of the GQD solutions under ambient light are shown in the insets of Figure 4d–f. Generally speaking, the use of low source concentration, short heating time, and low microwave power will lead to transparent or pale yellow GQD solution, which is composed of GQDs with diameters less than 10 nm. On the contrary, the GQD solution becomes dark brown which is composed of high density GQDs with diameters between 10 and 21 nm.

Figure 5a shows the photoluminescence (PL) spectra of the GQD solution. The solution was excited by a Xe lamp from the fluorescence spectrometer. A broad emission peak at 473 nm is observed when the sample is excited by 375 nm. The PL peak shifts from 473 to 519 nm when the excitation wavelength changed from 375 to 450 nm. However, the PL intensity decreases as

the PL peak red-shifted. The excitation wavelength dependence of the emission wavelength and intensity is a common phenomenon observed in carbon-based QDs.<sup>4,5,8–11</sup> Some suggested that emissive traps, electronic conjugate structures, and free zigzag sites are the reasons for the phenomenon.<sup>8–11</sup> However, the origin of the phenomenon in the GQDs could be related to the surface states which will be discussed later.

It is worth noting that the size-independent PL of the GQDs is observed as shown in Figure 5c. In agreement with the absorbance results (Figure 4d), the peak position of the emission PL does not change with the size of the GQDs. The size-independent PL of the GQDs could be related to the self-passivated layer of the GQDs. Figure 5d shows a series of GQD solutions irradiated by the ambient (top) and UV lamp (bottom). The solutions were prepared by various heating times. Although the size of the GQDs increases with heating time, the emission color of the solutions does not change obviously. The quantum yields (QYs) of the GQDs prepared at various microwave heating times were determined by employing an absolute quantum yield measurement method.<sup>32,33</sup> As shown in Figure S5 of SI, the QYs are in the range of 7–11%, which are slightly higher than the reported values (4–10%) of carbon QDs.<sup>4,34</sup>

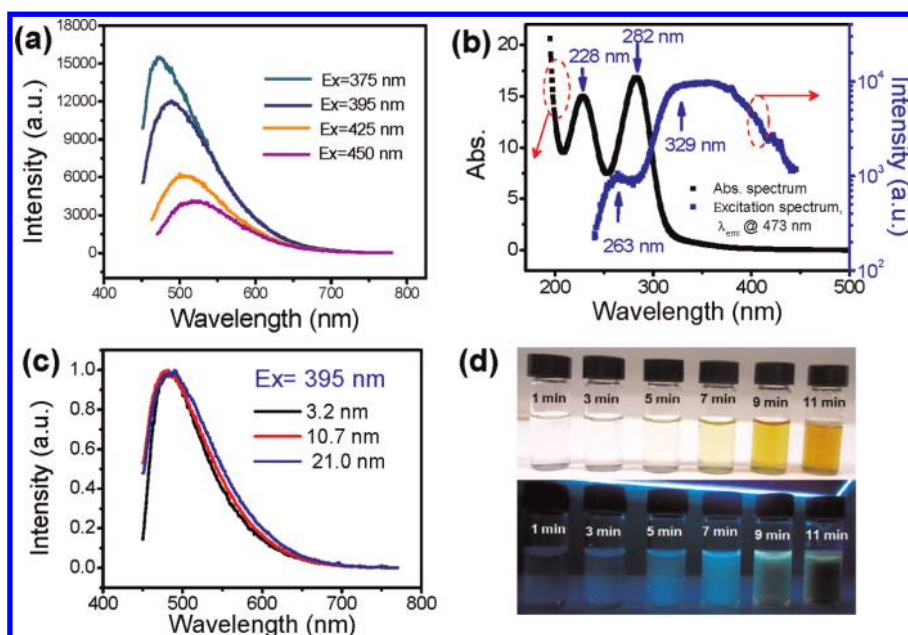


**Figure 5.** PL properties of the GQDs. (a) The PL spectra of the GQDs excited by various wavelengths; (b) the absorbance and excitation spectra of the GQDs solution; (c) the normalized PL spectra of the GQDs with various sizes; (d) the GQDs solutions irradiated by ambient light (top) and 365 nm UV lamp (bottom). The GQDs were prepared with 11.1 wt % glucose solution for 5 min (a and b), 5–9 min (c), 1–11 min (d) microwave heating at 595 W.

The photoluminescence excitation (PLE) spectrum of the GQDs was measured by monitoring the emission at 473 nm as shown in Figure 5b. The PLE spectrum shows two peaks centered at 263 and 329 nm, which are similar to the reported PLE peaks 257–270 nm and 320–331 nm of GQDs prepared by hydrothermal graphene oxide reduction method<sup>4</sup> and chemical exfoliation method.<sup>16</sup> The two PLE peaks at 263 and 329 nm should be related to two kinds of electron transitions.<sup>4,16</sup> It is worth noting that the energy difference between the two peaks (263 and 329 nm) in the PLE spectrum is  $\sim 1.0$  eV, which is equal to the energy difference in the two UV absorption peaks (228 and 282 nm).

Apart from visible light PL, UV emission of carbon QDs has been reported.<sup>35</sup> It was found that  $\sim 350$  nm (3.54 eV) UV emission was observed from carbon QDs with size of 1.2 nm. To observe the DUV PL emission of the GQDs as revealed by the absorbance spectrum, the samples were excited by 197 and 266 nm lasers. The samples were first spin-coated on SiO<sub>2</sub>/Si substrate (water evaporated) for DUV PL measurement. The DUV emission at 4.1 and 3.9 eV from the GQDs was observed for the first time when the sample was excited by 197 and 266 nm, respectively, as shown in Figure 6a. There are two emission peaks centered at 4.10 eV (303 nm) and 3.01 eV (412 nm) which are corresponding to DUV and blue emissions, respectively, when excited by 197 nm. The 4.10 eV peak is more intense than the 3.01 eV peak. The two emission peaks red-shift to 3.9 and 2.92 eV when excited by 266 nm. In addition, the 2.92 eV peak is more intense than the 3.9 eV peak, which is in contrast to the sample excited by 197 nm.

The observations are, however, consistent with the excitation wavelength dependence phenomenon in GQDs.

The time-resolved PL of the GQDs at 10 K was measured. The sample was excited at 266 nm. The typical luminescence decay for emission at 2.94 eV (422 nm) is shown in Figure 6b. The decay curve can be best fitted with a single-exponential function giving a lifetime  $\tau$  of 0.404 ns. However, most of the literature used a three-exponential function to fit the decay curve of GQDs.<sup>16,36</sup> For comparison, we also fitted the decay curve with a three-exponential function as shown in Figure 6b. It is found that the decay curve contains a fast component ( $\tau_1 = 0.283$  ns) and two slow components ( $\tau_2 = 3.66$  ns and  $\tau_3 = 6.29$  ns), which is consistent with the previous reports on lifetimes obtained from GQDs prepared by chemical exfoliation,<sup>16</sup> and carbon dots prepared by the electrochemical method.<sup>36</sup> The slow component lifetimes are suggested to be related to oxygen in the quantum dots.<sup>36</sup> The inset in Figure 6 b shows the PL spectrum of the GQDs at 10 K. The two emission peaks are blue-shifted slightly as compared to the sample at 300 K.

Since both the source (glucose) and solvent (DI water) do not exhibit DUV absorption and emission, the DUV emission should originate from the GQDs. The DUV emission of the self-passivated GQDs could be attributed to the  $\pi$  electron transition of C=C in the core of GQD which is composed of cyclic aromatic hydrocarbon-like structure. The self-passivated layer on the surface of the GQDs should play an important

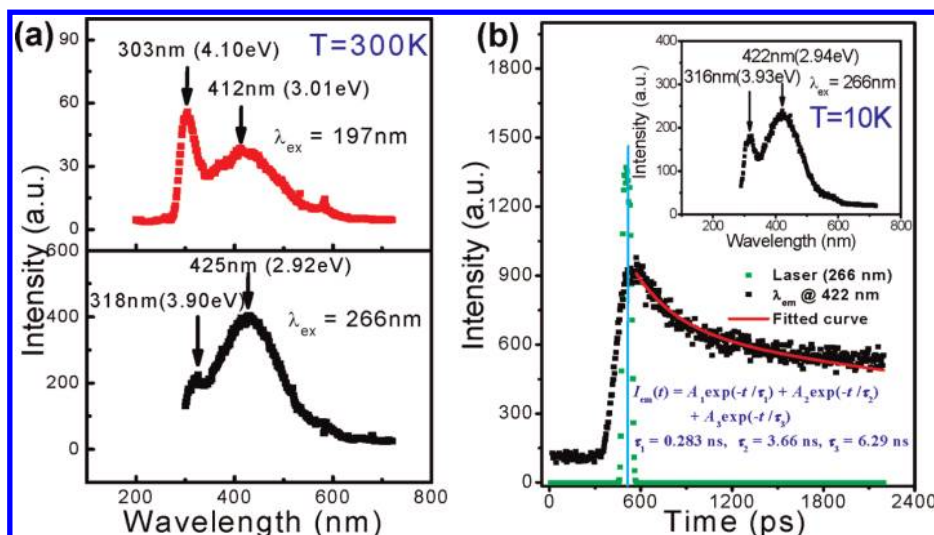


Figure 6. The deep UV emission spectra and the time-resolved PL of the GQDs: (a) PL spectra excited by 197 and 266 nm; (b) typical luminescence decay curve for the UV emission measured at 10 K, the inset is the corresponding PL spectrum. The GQDs were prepared with 11.1 wt % glucose solution for 5 min microwave heating at 595 W.

role in the observed DUV emission. As demonstrated above, our GQDs consist of C=C core, as well as O and H containing functional groups on the surface. The functional groups (C–OH, C=O, C–O–C, C–H) on the surface of the GQDs form “surface states” which are the energy levels between  $\pi$  and  $\pi^*$  states of C=C. Because of the difference in chemical bonding between C=C and C=O groups, the variation of  $\pi^*$  energy states is expected. Thus a distribution  $\pi^*$  band (C=C and C=O) is resulted. The absorption and emission transitions of the GQDs and their energy levels are shown in Figure S6 of SI. Both DUV (4.10 eV) and blue (3.01 eV) emissions are red-shifted as compared to their absorption energies. The surface states energy level can be estimated from the energy difference between the intrinsic absorption energy at 228 nm (5.44 eV) and the surface states absorption energy at 282 nm (4.40 eV), or the energy difference between the intrinsic emission at 303 nm (4.10 eV) and surface states emission at 412 nm (3.01 eV). The energy level of the surface states is determined to be  $\sim 1.0$  eV above  $\pi$  energy level of the GQDs. Based on the EELS, FTIR, and XPS results, different kinds of functional groups (C–OH, C=O, C–O–C, C–H) are presented on the surface of the GQD, forming “surface states” energy levels between  $\pi$  and  $\pi^*$  states of C=C. The functional groups have various energy levels, which may result in a series of emissive traps as shown in Figure S6 of SI. When a certain excitation wavelength illuminates the GQDs, a surface state emissive trap will dominate the emission. As the excitation wavelength changes, another corresponding surface state emissive trap will become dominant. Since both absorption and emission spectrum of the GQDs are independent of size, the emissive traps induced by surface states of the functional groups

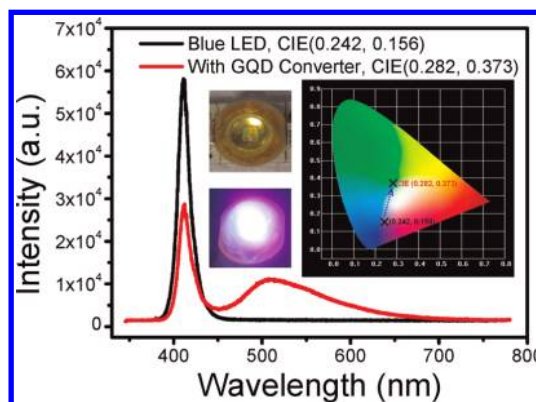


Figure 7. Color converter of the GQDs. Luminescence spectra of the blue LED with and without GQDs coating. Left inset: Photographs of the GQD coated LED without (top) and with applied voltage (bottom). Right inset: The CIE chromaticity coordinates for the illuminating blue LED with and without GQD layer.

should play an important role in the GQDs emission. This explains the excitation wavelength dependent phenomenon of the GQDs.

Since the GQDs exhibited relatively high QY, it should be an excellent light converter. To demonstrate the white light emission of the GQDs by converting blue light, a few drops of concentrated GQD solution (same as the sample shown in Figure 5a) were coated onto a commercially available blue light emitting diode (LED). After the water was evaporated by elevated temperature ( $\sim 100$  °C) for 5 min, a layer of the GQDs was formed on the surface of the LED. As shown in Figure 7, the uncoated blue LED emitted blue light centered at 410 nm. After coating the GQDs, the intensity of the blue light weakens, accompanied by the presence of a broad band peaked at  $\sim 510$  nm. The corresponding LED with and without applied voltage are shown in the left-hand side of the inset of Figure 7.

The applied voltage and current for the LED were 2.9 V and 10 mA, respectively. The Commission International d'Eclairage (CIE) chromaticity coordinates for illuminating blue LEDs with and without GQD coating are shown in the right-hand side of the inset of Figure 7. Clearly, with a GQD layer, the CIE chromaticity coordinates of the blue LED is shifted from (0.242, 0.156) to (0.282, 0.373), demonstrating that the GQDs are capable of converting blue light into white light. When excited by a blue LED of 410 nm, the GQDs will emit a broad band (fwhm = 104 nm) centered at 510 nm. Owing to the mixing of 410 nm and a broad emission peaked at 510 nm, the blue light is converted to white light. By tuning the growth parameters of the GQDs, the highly sought white LEDs with CIE (0.33, 0.33) for solid-state-lighting may be able to be obtained. The water-soluble GQDs exhibit excellent light converting properties as compared to compound-semiconductor-based QDs such as multishell-structured CdSe//ZnS/CdSZnS and CdSe/CdS/ZnS/CdSZnS QDs.<sup>37</sup> The nontoxic

nature and unique DUV emission from the GQDs will make this material promising for a wide range of optoelectronic devices.

## CONCLUSIONS

Highly luminescence GQDs prepared by a microwave-assisted hydrothermal method with the largest emission energy of 4.1 eV were observed. The emission wavelength of the GQDs is independent of the size of the GQDs, which is different from the carbon QDs prepared by conventional methods. The unique optical properties of the GQDs are attributed to the self-passivated layer which leads to the formation of surface states between the  $\pi^*$  band and  $\pi$  energy level. The quantum yields of the GQDs were determined to be 7–11%. The GQDs acting as an efficient light converter for converting blue light into white light was also demonstrated by coating GQDs onto a blue light emitting diode. The GQDs should find important potential applications in the fields of DUV photonic devices.

## METHODS

**Water-Soluble GQDs Preparation.** A series of glucose solutions with various concentrations (2.2, 4.4, 6.7, 8.9, 11.1 wt %) were prepared by using glucose and DI water as source and solvent, respectively. Glucose solutions of 2–2.5 mL were siphoned to a glass bottle with tightened cover. The volume of the glass bottle is 4 mL. The glass bottle was heated with a conventional microwave oven at a certain power (280, 336, 462, 595, and 700 W) for a period of time (1, 3, 5, 7, 9, and 11 min). It is found that the experimental parameters such as microwave power, heating time, source concentration, as well as solution volume have a distinct effect on the growth of GQDs; in turn we can use these parameters to prepare GQDs in a controllable way. In the process of microwave heating, the solution changes color (e.g., from transparent to pale yellow) as a result of formation of GQDs. Subsequently, the glass bottle was cooled to room temperature for characterizations. Besides glucose, we also investigated sucrose and fructose.

**Characterizations.** TEM, HRTEM, STEM, EDS, and EELS measurements were performed on JEOL, JEM-2100F at operating voltage of 200 kV. X-ray diffraction (XRD) was carried out with a Rigaku SmartLab X-ray diffractometer (Cu K $\alpha$  radiation  $\lambda$  = 1.54056 Å) operating at 45 kV and 200 mA. The height of the GQDs samples was characterized by atomic force microscope (AFM) (Digital Instruments NanoScope IV) operating in the tapping mode. The Fourier transform infrared (FTIR) spectra of the samples were obtained using the KBr pellet method by Nicolet Magna-IR 760 spectrometer with a resolution of 4 cm<sup>-1</sup>. XPS experiment was performed using Al K $\alpha$  source, having an energy of 1486.6 eV and at room temperature with the VG ESCALAB MKII. The UV–vis spectra were recorded at room temperature on a Shimadzu UV-2550 UV–vis spectrophotometer. For PL characterizations, the excitation and emission spectra of the GQDs solutions were recorded using an FLS920P Edinburgh Analytical Instrument apparatus with Xe lamp as an excitation source. The DUV emission spectra of the GQD films were investigated by employing a specially designed time-resolved DUV laser spectroscopy system consisting of a frequency tripled (266 nm) and quadrupled (197 nm) Ti-sapphire laser (100 fs) with a 76 MHz repetition rate. A streak camera with a time resolution of 2 ps was used for recording time-resolved PL.<sup>38</sup> The absolute quantum yield measurements were carried out using an integrating sphere (Edinburgh instruments,

150 mm in diameter-coated with barium sulfate). All the GQD samples were diluted with DI water to avoid reabsorption; the samples were placed in the cuvettes inside the integrating sphere. The spectra of the LEDs with and without GQD coating were recorded by an Ocean Optics USB4000 fiber optic spectrometer.

*Conflict of Interest:* The authors declare no competing financial interest.

*Acknowledgment.* This work was partially supported by the Research Grants Council of Hong Kong (Project No. PolyU 5013/09P), HK PolyU grants (Project Nos. G-XY3E and 1-ZV8N), the National Natural Science Foundation of China (Grant No. 61106098 and 61066004), and NSF under Grant No. DRM-0906879. J.H.X. acknowledges the support of Royal Society Kan Tong Po Visiting Professorships. H.X.J. and J.Y.L. would like to acknowledge the support of Whitacare endowed chair positions through the AT&T Foundation.

*Supporting Information Available:* Additional experimental results on TEM, HR-TEM, and AFM images of GQDs prepared under different conditions. This material is available free of charge via the Internet at <http://pubs.acs.org>.

## REFERENCES AND NOTES

1. Trauzettel, B.; Bulaev, D. V.; Loss, D.; Burkard, G. Spin Qubits in Graphene Quantum Dots. *Nat. Phys.* **2007**, *3*, 192–196.
2. Güçlü, A.; Potasz, P.; Hawrylak, P. Electric-field Controlled Spin in Bilayer Triangular Graphene Quantum Dots. *Phys. Rev. B* **2011**, *84*, 035425.
3. Ritter, K. A.; Lyding, J. W. The Influence of Edge Structure on the Electronic Properties of Graphene Quantum Dots and Nanoribbons. *Nat. Mater.* **2009**, *8*, 235–242.
4. Pan, D.; Zhang, J.; Li, Z.; Wu, M. Hydrothermal Route for Cutting Graphene Sheets into Blue-Luminescent Graphene Quantum Dots. *Adv. Mater.* **2010**, *22*, 734–738.
5. Shen, J.; Zhu, Y.; Chen, C.; Yang, X.; Li, C. Facile Preparation and Upconversion Luminescence of Graphene Quantum Dots. *Chem. Commun.* **2011**, *47*, 2580–2582.
6. Zhang, Z. Z.; Chang, K. Tuning of Energy Levels and Optical Properties of Graphene Quantum Dots. *Phys. Rev. B* **2008**, *77*, 235411.

7. Gupta, V.; Chaudhary, N.; Srivastava, R.; Sharma, G. D.; Bhardwaj, R.; Chand, S. Luminescent Graphene Quantum Dots for Organic Photovoltaic Devices. *J. Am. Chem. Soc.* **2011**, *133*, 9960–9963.
8. Liu, R.; Wu, D.; Feng, X.; Müllen, K. Bottom-Up Fabrication of Photoluminescent Graphene Quantum Dots with Uniform Morphology. *J. Am. Chem. Soc.* **2011**, *133*, 15221–15223.
9. Li, Y.; Hu, Y.; Zhao, Y.; Shi, G.; Deng, L.; Hou, Y.; Qu, L. An Electrochemical Avenue to Green-Luminescent Graphene Quantum Dots as Potential Electron-Acceptors for Photovoltaics. *Adv. Mater.* **2011**, *23*, 776–780.
10. Zhu, S.; Zhang, J.; Qiao, C.; Tang, S.; Li, Y.; Yuan, W.; Li, B.; Tian, L.; Liu, F.; Hu, R.; *et al.* Strongly Green-Photoluminescent Graphene Quantum Dots for Bioimaging Applications. *Chem. Commun.* **2011**, *47*, 6858–6860.
11. Shen, J.; Zhu, Y.; Yang, X.; Zong, J.; Zhang, J.; Li, C. One-Pot Hydrothermal Synthesis of Graphene Quantum Dots Surface-Passivated by Polyethylene Glycol and their Photoelectric Conversion under Near-Infrared Light. *New J. Chem.* **2011**, c1nj20658c.
12. Pan, D.; Guo, L.; Zhang, J.; Xi, C.; Xue, Q.; Huang, H.; Li, J.; Zhang, Z.; Yu, W.; Chen, Z.; *et al.* Cutting  $sp^2$  Clusters in Graphene Sheets into Colloidal Graphene Quantum Dots with Strong Green Fluorescence. *J. Mater. Chem.* **2012**, *22*, 3314–3318.
13. Lu, J.; Yeo, P. S. E.; Gan, C. K.; Wu, P.; Loh, K. P. Transforming  $C_{60}$  Molecules into Graphene Quantum Dots. *Nat. Nanotechnol.* **2011**, *6*, 247–252.
14. Yan, X.; Cui, X.; Li, L. Synthesis of Large, Stable Colloidal Graphene Quantum Dots with Tunable Size. *J. Am. Chem. Soc.* **2010**, *132*, 5944–5945.
15. Yan, X.; Cui, X.; Li, B.; Li, L. Large, Solution-Processable Graphene Quantum Dots as Light Absorbers for Photovoltaics. *Nano Lett.* **2010**, *10*, 1869–1873.
16. Peng, J.; Gao, W.; Gupta, B. K.; Liu, Z.; Romero-Aburto, R.; Ge, L.; Song, L.; Alemany, L. B.; Zhan, X.; Gao, G.; *et al.* Graphene Quantum Dots Derived from Carbon Fibers. *Nano Lett.* **2012**, *12*, 844–849.
17. Schnez, S.; Molitor, F.; Stampfer, C.; Güttinger, J.; Shorubalko, I.; Ihn, T.; Ensslin, K. Observation of Excited States in a Graphene Quantum Dot. *Appl. Phys. Lett.* **2009**, *94*, 012107.
18. Zhu, H.; Wang, X.; Li, Y.; Wang, Z.; Yang, F.; Yang, X. Microwave Synthesis of Fluorescent Carbon Nanoparticles with Electrochemiluminescence Properties. *Chem. Commun.* **2009**, 5118–5120.
19. Wang, X.; Qu, K.; Xu, B.; Ren, J.; Qu, X. Microwave Assisted One-Step Green Synthesis of Cell-Permeable Multicolor Photoluminescent Carbon Dots without Surface Passivation Reagents. *J. Mater. Chem.* **2011**, *21*, 2445–2450.
20. Oshima, C.; Nagashima, A. Ultra-Thin Epitaxial Films of Graphite and Hexagonal Boron Nitride on Solid Surfaces. *J. Phys.: Condens. Matter* **1997**, *9*, 1–20.
21. Biedermann, L.; Bolen, M.; Capano, M.; Zemlyanov, D.; Reifemberger, R. Insights into Few-Layer Epitaxial Graphene Growth on 4H-SiC(0001) Substrates from STM Studies. *Phys. Rev. B* **2009**, *79*, 125411.
22. Ci, L.; Song, L.; Jin, C.; Jariwala, D.; Wu, D.; Li, Y.; Srivastava, A.; Wang, Z. F.; Storr, K.; Balicas, L.; *et al.* Atomic Layers of Hybridized Boron Nitride and Graphene Domains. *Nat. Mater.* **2010**, *9*, 430–435.
23. Dato, A.; Radmilovic, V.; Lee, Z.; Phillips, J.; Frenklach, M. Substrate-Free Gas-Phase Synthesis of Graphene Sheets. *Nano Lett.* **2008**, *8*, 2012–2016.
24. Urquhart, S. G.; Smith, A. P.; Ade, H. W.; Hitchcock, A. P.; Rightor, E. G.; Lidy, W. Near-Edge X-ray Absorption Fine Structure Spectroscopy of MDI and TDI Polyurethane Polymers. *J. Phys. Chem. B* **1999**, *103*, 4603–4610.
25. Luo, Z.; Lu, Y.; Somers, L. A.; Charlie Johnson, A. T. High Yield Preparation of Macroscopic Graphene Oxide Membranes. *J. Am. Chem. Soc.* **2009**, *131*, 898–899.
26. Alivisatos, A. P. Semiconductor Clusters, Nanocrystals, and Quantum Dots. *Science* **1996**, *271*, 933–937.
27. Guzelian, A. A.; Banin, U.; Kadavanich, A. V.; Peng, X.; Alivisatos, A. P. Colloidal Chemical Synthesis and Characterization of InAs Nanocrystal Quantum Dots. *Appl. Phys. Lett.* **1996**, *69*, 1432–1434.
28. Micić, O.; Cheong, H.; Fu, H.; Zunger, A.; Sprague, J.; Mascarenhas, A.; Nozik, A. Size-Dependent Spectroscopy of InP Quantum Dots. *J. Phys. Chem. B* **1997**, *101*, 4904–4912.
29. Cademartiri, L.; Montanari, E.; Calestani, G.; Migliori, A.; Guagliardi, A.; Ozin, G. A. Size-Dependent Extinction Coefficients of PbS Quantum Dots. *J. Am. Chem. Soc.* **2006**, *128*, 10337–10346.
30. Moreels, I.; Lambert, K.; Muynck, D.; De; Vanhaecke, F.; Poelman, D.; Martins, J. C.; Allan, G.; Hens, Z. Composition and Size-Dependent Extinction Coefficient of Colloidal PbSe Quantum Dots. *Chem. Mater.* **2007**, *19*, 6101–6106.
31. Keuleyan, S.; Lhuillier, E.; Brajuskovic, V.; Guyot-Sionnest, P. Mid-infrared HgTe Colloidal Quantum Dot Photodetectors. *Nat. Photon.* **2011**, *5*, 489–493.
32. Reineke, S.; Lindner, F.; Schwartz, G.; Seidler, N.; Walzer, K.; Lüssem, B.; Leo, K. White Organic Light-Emitting Diodes with Fluorescent Tube Efficiency. *Nature* **2009**, *459*, 234–239.
33. de Mello, J. C.; Wittmann, H. F.; Friend, R. H. An Improved Experimental Determination of External Photoluminescence Quantum Efficiency. *Adv. Mater.* **1997**, *9*, 230–232.
34. Sun, Y. P.; Zhou, B.; Lin, Y.; Wang, W.; Fernando, K. A. S.; Pathak, P.; Meziani, M. J.; Harruff, B. A.; Wang, X.; Wang, H. Quantum-Sized Carbon Dots for Bright and Colorful Photoluminescence. *J. Am. Chem. Soc.* **2006**, *128*, 7756–7757.
35. Li, H.; He, X.; Kang, Z.; Huang, H.; Liu, Y.; Liu, J.; Lian, S.; Tsang, C. H. A.; Yang, X.; Lee, S. T. Water-Soluble Fluorescent Carbon Quantum Dots and Photocatalyst Design. *Angew. Chem., Int. Ed.* **2010**, *49*, 4430–4434.
36. Bao, L.; Zhang, Z. L.; Tian, Z. Q.; Zhang, L.; Liu, C.; Lin, Y.; Qi, B. P.; Pang, D. W. Electrochemical Tuning of Luminescent Carbon Nanodots: From Preparation to Luminescence Mechanism. *Adv. Mater.* **2011**, *23*, 5801–5806.
37. Jang, E.; Jun, S.; Jang, H.; Lim, J.; Kim, B.; Kim, Y. White-Light-Emitting Diodes with Quantum Dot Color Converters for Display Backlights. *Adv. Mater.* **2010**, *22*, 3076–3080.
38. Nam, K. B.; Nakarmi, M. L.; Li, J.; Lin, J. Y.; Jiang, H. X. Photoluminescence Studies of Si-Doped AlN Epilayers. *Appl. Phys. Lett.* **2003**, *83*, 2787–2789.